Masses of high-z galaxy hosting haloes from angular clustering and their evolution in the CDM model[*]

Takashi Hamana[1], Toru Yamada[1], Masami Ouchi[2,3], Ikuru Iwata[4],
Tadayuki Kodama[1,5]

[1] *National Astronomical Observatory of Japan, Mitaka, Tokyo 181-8588, Japan*
[2] *Space Telescope Science Institute, 3700 San Martin Drive, Baltimore, MD 21218, USA*
[3] *Hubble Fellow*
[4] *Okayama Attrophysical Observatory, National Astronomical Observatory of Japan, Kamogata, Okayama 719-0232, Japan*
[5] *European Southern Observatory, Karl-Schwarzschild-Str. 2, D-85748, Garching, Germany*

ABSTRACT

We examine masses of hosting haloes of two photometrically-selected high-z galaxy samples: the old passively-evolving galaxies (OPEGs) at $z \sim 1$ and Lyman Break Galaxies (LBGs) at $z \sim 4$ both taken from the Subaru/XMM-Newton Deep Survey (SXDS). The large survey area of the SXDS (1 deg^2) allows us to measure the angular two-point correlation functions to a wide separation of > 10 arcmin with a good statistical quality. We utilize the halo model prescription for estimating characteristic masses of hosting haloes from the measured large-scale clustering amplitudes. It is found that the hosting halo mass positively correlates with the luminosity of galaxies. Then, adopting the extended Press-Schechter model (EPS), we compute the predictions for the mass evolution of the hosting haloes in the framework of the cold dark matter (CDM) cosmology in order to make an evolutionary link between the two galaxy samples at different redshifts and to identify their present-day descendants by letting their haloes evolve forward in time. It is found that, in the view of the mass evolution of hosting haloes in the CDM model, bright ($i' \lesssim i'_* + 1$) LBGs are consistent with being the progenitor of the OPEGs, whereas it is less likely that the LBG population, as a whole, have evolved into the OPEG population. It is also found that the present-day descendants of both the bright LBGs and OPEGs are likely to be located in massive systems such as groups of galaxies or clusters of galaxies. Finally, we estimate the hosting halo mass of local early-type galaxy samples from the 2dF and SDSS based on the halo model and it turns out that their expected characteristic mass of hosting haloes is in good agreement with the EPS predictions for the descendant's mass of both the bright LBGs and OPEGs.

Key words: galaxies: formation — galaxies: haloes — galaxies: high-redshift — cosmology: theory — dark matter

1 INTRODUCTION

Galaxies consist of two major ingredients, namely, the baryonic and dark matter. There are pieces of observational evidence that properties and evolution of the baryonic component are not independent of those of the dark matter, but are closely correlated. For instance, early/late type galaxies dominate the bright/faint part of the galaxy luminosity function, which suggests that the star formation history and/or morphology are related to the total mass of the system, provided that the luminosity is basically proportional to the total mass. Another example is the morphology-density relation (Dressler 1980; Postman & Geller 1984), which may indicate the possible influence of the mass of hosting halo on the galaxy formation on group/cluster scale as well. It follows from these pieces of evidence that the mass of the hosting halo could be one of the most fundamental quantities in the galaxy formation. Therefore, in order to understand the galaxy formation, the evolution of baryonic and dark matter should not be treated as independent processes but should be investigated in a unified way.

---

[*] Based on data collected at Subaru Telescope, which is operated by the National Astronomical Observatory of Japan.

The baryonic contents (stars and gas) of galaxies have been well studied by both photometric and spectroscopic observations and have been extensively analyzed with a help of well developed theoretical tools such as stellar population synthesis models (e.g., Bruzual & Charlot 2003). On the other hand, the dark matter component of hosting halos has been less studied observationally due to the technical difficulties in probing it since it requires dynamical tracers or gravitational lensing. Theoretical models for the evolution of dark matter, however, have been well developed with numerical simulations and analytical models such as Press-Schechter prescriptions (Press & Schechter 1974).

It has been known that a large-scale clustering amplitude of galaxies provides a unique way of estimating their hosting halo mass in a statistical manner. This makes use of a finding from theoretical studies of dark-matter structure formation in the cold dark matter (CDM) model that a clustering amplitude of dark matter haloes depends monotonically and strongly on the halo mass (Mo & White 1996). By measuring the clustering amplitude of galaxy populations selected from a wide-field survey, we can relate properties of the populations such as stellar mass and/or star formation rate with the mass of their hosting halo (e.g., Giavalisco & Dickinson 2001; Adelberger et al. 2005). It, in turn, enables us to explore an ancestor–descendant connection of different galaxy populations at various redshifts from the viewpoints of both the star formation and the dark matter assembly (Moustakas & Somerville 2002; Hamana et al. 2004; Ouchi et al 2004b).

This approach is exactly the one we take, in what follows, to explore the evolution of the old passively-evolving galaxies (OPEGs) at $z \sim 1$ and Lyman Break Galaxies (LBGs) at $z \sim 4$. The OPEGs are selected by optical colour criteria (see §3.1) being consistent with a passively evolving galaxy with the major star-formation epoch at $z > 2$. Since the age of the universe at $z = 2$ is only $\sim 2.3h^{-1}$Gyrs, progenitors of the OPEGs must have experienced an active star formation phase at some high redshifts of $z > 2$. The LBGs, which are in general actively star forming galaxies at high redshifts, are naturally a strong candidate of a major population of the progenitor of such OPEGs. While there is a fraction of dusty star-forming galaxies or red old galaxies with little star formation, which are not selected by the LBG criteria at $z \sim$2–2.5 (e.g., Franx et al. 2003; Reddy et al. 2005), LBGs are still most populous among them. In addition, the OPEGs are considered as strong candidates for progenitors of the present-day early-type galaxies since the simple passive evolution in their stellar populations can easily link between them. We examine relations between the two galaxy populations in terms of the evolution of hosting dark matter haloes. Our primary question addressed in this paper is *"supposing the LBGs are a major progenitor of the OPEGs, are their hosting halo masses compatible with the mass evolution of dark matter haloes in the CDM structure formation model ?"* Also, we discuss possible present-day descendants of those high-z galaxies from the viewpoint of the masses of hosting haloes.

We determine the clustering amplitude at large scales with angular two-point correlation functions of the OPEGs and LBGs measured, with a good accuracy, from a wide field (1 deg^2) deep imaging data-set of Subaru/XMM-Newton Deep Survey (SXDS). Multi-band colour selection techniques successfully isolate those galaxies with well calibrated redshift selection functions, which enable us to compute an accurate prediction for the corresponding dark matter angular correlation function via the Limber's projection. This large data-set and selection techniques allow us to compute a large-scale galaxy bias in a robust manner. Comparing the measured large-scale bias with the ones predicted by the halo model, we place a limit on the hosting halo mass of galaxy populations. Here we adopt an empirically parameterized model for the halo occupation function (HOF) which describes statistical relations between galaxies and their hosting haloes. Then, utilizing the extended Press-Schechter (EPS) prescriptions, we examine the evolution of halo mass in the framework of the CDM model. In this way, we compare hosting halo masses of each galaxy population at different redshift, and explore their connection.

The outline of this paper is as follows. Section 2 describes models and basic equations. Section 3 summarizes observational data that are used to place a constraint on the hosting halo mass. Results are presented in section 4. Finally, section 5 is devoted to a summary and discussion.

Throughout this paper, we adopt a flat ΛCDM cosmology with the matter density $\Omega_{\mathrm{m}} = 0.3$, the cosmological constant $\Omega_{\Lambda} = 0.7$, the Hubble constant $H_0 = 100h$ km s^{-1} Mpc^{-1} with $h = 0.7$, and the normalization of the matter power spectrum $\sigma_8 = 0.9$. We adopt the fitting function of the CDM power spectrum of Bardeen et al. (1986). We present magnitudes in the AB system.

2 MODELS

2.1 Dark matter angular correlation function

We quantify a clustering amplitude of a population of galaxies by comparing their angular two-point correlation function with the corresponding dark matter correlation function. Let $q(z)$ be a normalized redshift selection function of a population of galaxies being considered, the dark matter angular two-point correlation function is computed from the dark matter power spectrum (P_{DM}) via the Limber projection (see e.g, chapter 2 of Bartelmann & Schneider 2001):

$$\omega_{DM}(\theta) = \int dr \, q^2(r) \int \frac{dk}{2\pi} k \, P_{\mathrm{DM}}(k, r) \, J_0[f_K(r)\theta k], \quad (1)$$

where $J_0(x)$ is the zeroth-order Bessel function of the first kind. For the spatially flat cosmology ($\Omega_{\mathrm{m}} + \Omega_{\Lambda} = 1$) as we consider throughout the present paper, the radial function $f_K(r)$ is equivalent to r, and $r = r(z)$ is the radial comoving distance given by $r(z) = c/H_0 \int_0^z dz' \, [\Omega_{\mathrm{m}}(1+z')^3 + \Omega_{\Lambda}]^{-1/2}$. We use the nonlinear fitting function of the CDM power spectrum by Peacock & Dodds (1996).

2.2 Halo model

We utilize the halo model approach for estimating a characteristic mass of hosting haloes from the measured clustering amplitude of galaxies. Here, we summarize several expressions which are most relevant to the current analysis. See Hamana et al. (2004; and references therein) for details of the halo model.

We adopt a simple parametric form for the average

number of a given galaxy population as a function of the hosting halo mass:

$$N_{\rm g}(M) = \begin{cases} (M/M_1)^\alpha & (M > M_{min}) \\ 0 & (M < M_{min}) \end{cases},$$ (2)

which is characterized by the three parameters: The minimum mass of haloes which host the population of galaxies (M_{min}), a normalization parameter which can be interpreted as the critical mass above which haloes typically host more than one galaxy (M_1), and the power-law index of the mass dependence of the galaxy occupation number (α). For the dependences of the HOF parameters on the shape of the two-point correlation function, see Hamana et al. (2004; and references therein).

We introduce the average mass of hosting halo (weighted by the number of member galaxy) by

$$\langle M_{\rm host} \rangle = \frac{\int dM \; M \; N_{\rm g}(M) n_{\rm halo}(M)}{\int dM \; N_{\rm g}(M) n_{\rm halo}(M)},$$ (3)

where $n_{\rm halo}(M)$ denotes the halo mass function for which we adopt the fitting function of Sheth & Tormen (1999)

Since the halo model assumes the linear halo bias (Mo & White 1996) and $N_{\rm g}(M)$ solely depends on the halo mass, the galaxy bias on large scales (the scales larger than the virial radius of hosting haloes) is given by the galaxy number weighted halo bias:

$$b_{g,L} = \frac{\int dM \; b_{\rm halo}(M) N_{\rm g}(M) n_{\rm halo}(M)}{\int dM \; N_{\rm g}(M) n_{\rm halo}(M)},$$ (4)

where $b_{\rm halo}(M)$ is the halo bias, for which we adopt the fitting function of Sheth & Tormen (1999). Note that $b_{g,L}$ does not depend on M_1 but only on M_{min} and α.

Since galaxies considered in the following sections are distributed over a redshift interval, we take into account the redshift evolution of a quantity $X(z)$ (represents for $b_{g,L}^2$ or $\langle M_{\rm host} \rangle$) by computing its redshift average:

$$X \equiv \frac{\int dz \; [dV/dz] \; q(z)^k X(z)}{\int dz \; [dV/dz] \; q(z)^k},$$ (5)

where $k = 1$ for $\langle M_{\rm host} \rangle$ while $k = 2$ for $b_{g,L}^2$, and dV/dz denotes the comoving volume element per unit solid angle: $dV/dz = c/H_0 \; r^2 \; [\Omega_{\rm m}(1+z)^3 + \Omega_\Lambda]^{-1/2}$, again for the spatially flat cosmology.

2.3 Extended Press-Schechter model

The extended Press-Schechter (EPS) formalism was developed by Bond et al. (1991), Bower (1991) and Lacey & Cole (1993). Since the EPS model provides a way to treat halo mergers, which play an important role in the structure formation in the hierarchical CDM model, it has been widely applied to analytical and semi-analytical studies of the structure formation. We utilize the EPS model for making a statistical estimate of growth of halo masses. A key expression for this is the conditional probability $P_2(M_{t2}, z_2|M_{t1}, z_1)$ that a material in a halo of mass M_{t1} at z_1 will be in a halo of mass M_{t2} ($M_{t2} > M_{t1}$) at a later redshift z_2, leading to an expression for the conditional mass function $n_2(M_{t2}, z_2|M_{t1}, z_1)$.

Here we summarize only expressions which are directly

relevant to our analysis, see above references for their derivation. Let δ_c and σ be the critical density threshold for a spherical perturbation to collapse and the RMS density fluctuation smoothed over a region enclosing a mass M, respectively, the conditional probability is

$$P_2(M_{t2}, z_2|M_{t1}, z_1)dM_{t2}$$
$$= \frac{1}{\sqrt{2\pi}} \frac{\delta_{c2}(\delta_{c1} - \delta_{c2})}{\delta_{c1}} \left[\frac{\sigma_1^2}{\sigma_2^2(\sigma_1^2 - \sigma_2^2)} \right]^{3/2}$$
$$\times \exp\left[-\frac{(\sigma_2^2 \delta_{c1} - \sigma_1^2 \delta_{c2})^2}{2\sigma_1^2 \sigma_2^2 (\sigma_1^2 - \sigma_2^2)} \right] \left| \frac{d\sigma_2^2}{dM_{t2}} \right| dM_{t2},$$ (6)

where the subscripts 1 and 2 stand for epochs z_1 and z_2, respectively. The conditional mass function is given from this by

$$n_2(M_{t2}, z_2|M_{t1}, z_1)dM_{t2} \propto \frac{1}{M_{t2}} P_2(M_{t2}, z_2|M_{t1}, z_1)dM_{t2}.$$ (7)

3 DATA

We use two samples of photometrically-selected galaxies from B, R, i' and z' imaging data of the Subaru/XMM-Newton Deep Survey[1] (SXDS). The limiting magnitudes for the 3σ detection of an object in a 2 arcsec diameter aperture are $B \simeq 28.3$, $R \simeq 27.6$, $i' \simeq 27.5$ and $z' \simeq 26.5$ (Furusawa et al. in preparation). The seeing size of those images is $\sim 0.8''$. We avoid the edges of the field and the area affected by bright sources. The final effective area used in this paper is ~ 1 deg^2.

Below we summarize basic properties of the two galaxy samples, and present angular two-point correlation functions of those galaxies.

3.1 Old passively-evolving galaxies at $z \sim 1$

The photometric properties of the old passively-evolving galaxies (OPEGs) in the SXDS fields are presented in Kodama et al. (2004) and Yamada et al. (2005). For the sample selection of OPEGs, we follow the definition of Yamada et al. (2005) which imposes the two criteria: $0.8 < i' - z' < 1.2$ and $-0.05z' + 3.01 < R - z' < -0.03z' + 2.49$, on the z'-band selected catalog. This criteria effectively isolate the galaxies with star-formation epoch greater than $z_f > 2$ and located at $0.9 < z < 1.1$. This photometrically-selected sample is composed of 4,118 OPEG candidates with $z' < 25.0$ distributed in the effective area of 1.03 deg^2. It is found from the spectroscopic observations for the 93 OPEG candidates with $19 < z' < 22$ that the 73 objects lie between $z = 0.87$ and 1.12, and the 4 objects lie outside of the redshift interval, and the remaining 16 objects have undetermined redshift because of no usable feature in the spectrum or a poor S/N. Figure 8 of Yamada et al. (2005) shows the redshift distribution function of OPEGs obtained from the spectroscopically-identified objects. The contamination fraction is estimated to be between 0.05 (=4/[73+4]) and 0.22 (=20/93). We assume the contamination fraction of $f_C = 0.1$ in the following analyses. The luminosity function is well fitted by the

---

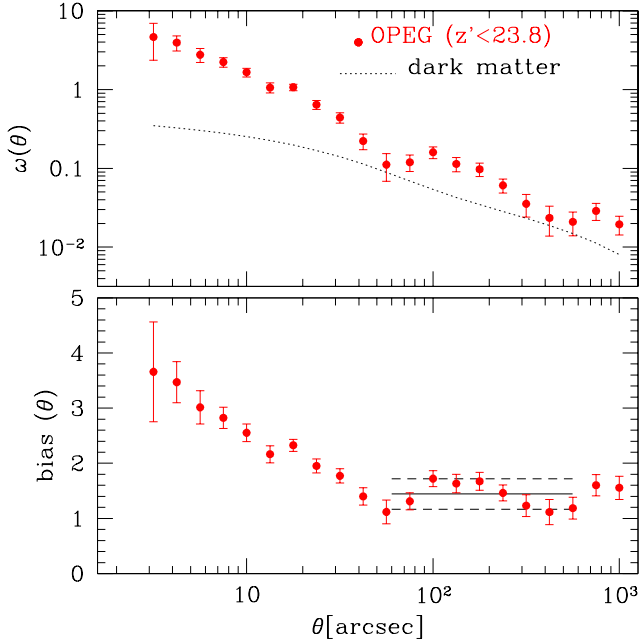[1] See http://www.naoj.org/Science/SubaruProject/SDS/ for details of the SXDS project.

Figure 1. *Upper panel*: Filled circles with error bars show the angular two-point correlation function for OPEGs with $z' < 23.8(= z'_* + 2)$. Note that the plotted correlation function has been corrected for the contamination (see text). The dotted line shows the CDM model prediction for the dark matter angular two-point correlation function computed via equation (1), where the nonlinear fitting function for the CDM power spectrum by Peacock & Dodds (1996) is used. *Lower panel*: The corresponding galaxy bias defined by equation (8) is plotted. The horizontal solid line shows the large-scale bias factor computed averaging the bias over an interval $1' < \theta < 10'$, and the dashed lines show its 1-σ error.

Schechter function with $\phi_* = (4.26 \pm 0.42) \times 10^{-3} h^3 \text{Mpc}^{-3}$, $\alpha_{LF} = -0.67 \pm 0.07$ and $M_{B*} = -21.38 \pm 0.10$ (Yamada et al. 2005). The latter magnitude corresponds to $z'_* = 21.8$ at $z = 1$.

The angular two-point correlation functions are computed using the pair-count estimator formulated by Landy & Szalay (1993): $\omega_g(\theta) = [DD(\theta) - 2DR(\theta) + RR(\theta)]/RR(\theta)$. In so doing, we distribute the same number of random samples with the same geometrical constraint as of the data sample. We repeat 100 random re-samplings, and the mean and RMS among the 100 measurements are taken as the mean correlation signal and 1-σ error. The effect of the contamination on the two-point correlation function is corrected by multiplying by a factor of $1/(1 - f_C)^2$, where the contaminants are assumed to be randomly distributed. A measured angular correlation function is plotted in the top panel of Figure 1 together with the dark-matter angular correlation function computed with the same redshift selection function. Note that the integral constraint (Groth & Peebles 1977) is estimated to be $\sim 7 \times 10^{-3}$ for a single power-law model $[\omega_g(\theta) \propto \theta^\beta]$ with the power-law index of $\beta = -1$, we may thus ignore an effect of a finite field size as far as $\theta < 10'$ is concerned.

We define the galaxy bias by

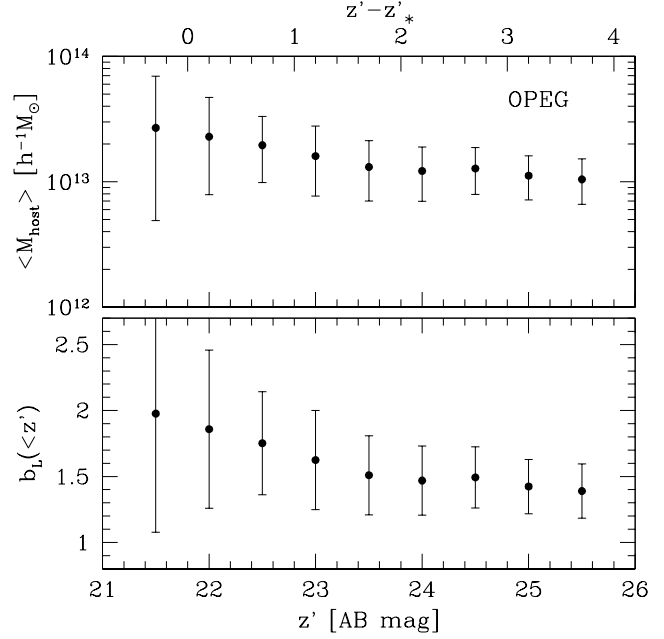$$b(\theta) = \sqrt{\frac{\omega_g(\theta)}{\omega_{DM}(\theta)}}, \qquad (8)$$

Figure 2. *Lower panel*: The large-scale bias factor (see test for the definition) for the OPEGs as a function of limiting magnitude. *Upper panel*: $\langle M_{\text{host}} \rangle$ computed from the halo model (with a fixed $\alpha = 0.8$) for the corresponding large-scale bias factor (see §4 for details). The upper abscissa axis indicates the magnitude difference from the z'_* value.

and is plotted in the bottom panel of Figure 1. As is shown there, on scales below ~ 1 arcmin, the bias decreases with the separation, while on larger scales it flattens. The comoving angular length of the transition scale ($\sim 1'$) is $\sim 0.7 h^{-1} \text{Mpc}$ (at $z = 1$) which corresponds to the virial radius of the halo with the mass $\sim 2 \times 10^{13} h^{-1} M_\odot$ at $z = 1$. This mass coincides with the characteristic mass of the hosting halo ($\langle M_{\text{host}} \rangle$) predicted by the halo model analysis in the next section. It may follow from this that the shape of the bias function is basically understood by the standard halo model picture: The small-scale clustering arises from galaxy pairs located in the same halo, while the large-scale clustering arises from galaxy pairs located in two different haloes.

Since the measured bias flattens on large-scales as expected by the halo model, we define the large-scale bias factor (b_L) as an averaged bias over $1' < \theta < 10'$ (illustrated in the bottom panel of Figure 1). We compute the large-scale bias factor for OPEG samples with different limiting magnitudes and show in the bottom panel of Figure 2. Broadly speaking, the large-scale bias factor is a decreasing function of the magnitude, though the significance is not high due to large error bars.

Let us devote, in passing, a little space to compare our measurement with previous studies. We derive the comoving correlation length, r_0, from the power-law fitting model of the angular two-point correlation function with the Limber equation (Peebles 1980). The correlation length r_0 is the normalization of the spatial two-point correlation function, $\xi = (r/r_0)^{-\gamma}$, where γ is related by $\gamma = \beta + 1$. We find $r_0 = 4.7 \pm 0.3 h^{-1} \text{Mpc}$ and $5.7 \pm 0.2 h^{-1} \text{Mpc}$ with the best-fit beta ($\beta = 1.1$) and the fixed beta ($\beta \equiv 0.8$), respectively.
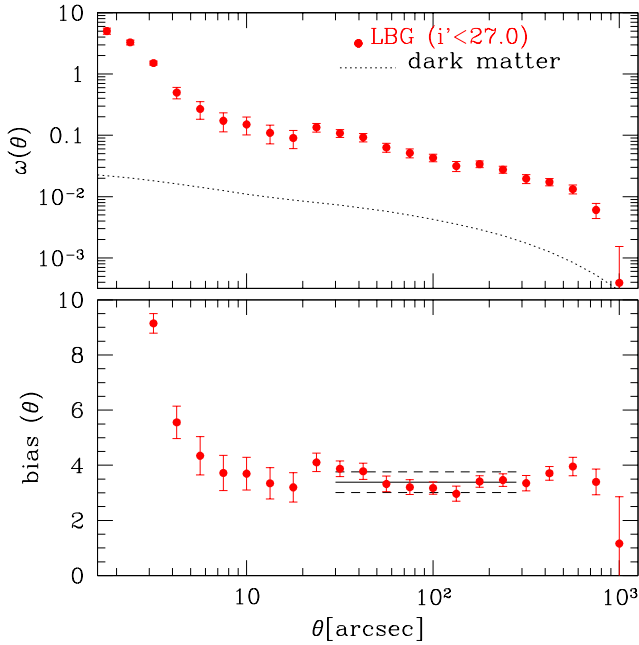
Figure 3. Same as Figure 1 but for the LBGs with $i' < 27.0 (= i'_* + 2)$.

Figure 4. Same as Figure 2 but for the LBGs.

This is consistent with $r_0 = 5.0 \pm 0.3 h^{-1} \mathrm{Mpc}$ obtained from $(R-I)$ colour selected red galaxies ($I = 18-24$) at $z \sim 0.85$ most of which have early-type spectra (Coil et al. 2004). In contrast, it is much smaller than $r_0 = (8-13) h^{-1} \mathrm{Mpc}$ obtained from (optical−NIR) colour selected "Extremely Red Objects" (EROs) at $1 \lesssim z \lesssim 2$ (Daddi et al 2001; McCarthy et al. 2001; Firth et al. 2002; Roche et al. 2002; Miyazaki et al. 2003). The luminosity segregation of clustering may not explain the difference of r_0, since, if we assume an early-type spectrum, the limiting magnitudes of their ERO searches reach to a comparable depth to our OPEG sample ($z' < 23.8$). The reason for the significant difference in r_0 is not clear. Coil et al. (2004) suggest that their red galaxies selected in optical bands may be a less-extreme version of EROs. Another possible reason would be an intrinsic evolution in the clustering strength due to the difference in redshift ranges of the samples. While our sample and Coil et al.'s (2004) sample are both limited to the small redshift range at $z \sim 1$, other "$R - K$" or "$I - K$" EROs samples have much wider range in redshift up to $z \sim 2$ The clustering strength of the red galaxies can evolve strongly between $z \sim 2$ and 1. Furthermore, the SXDS survey probes much larger volume than the other surveys and the effect of field-to-field variation is expected to relatively small. Further investigating into the origin of the difference is, however, beyond the scope of this paper, and we leave it for a future work.

3.2 Lyman break galaxies at $z \sim 4$

The sample selection and clustering properties of the Lyman break galaxies (LBGs) at $z \sim 4$ are described in Ouchi et al. (2005). Briefly, the LBGs are selected from i'-band selected catalog by three criteria: $B - R > 1.2$, $R - i' < 0.7$ and $B - R > 1.6(R - i') + 1.9$. The number counts of this sam-
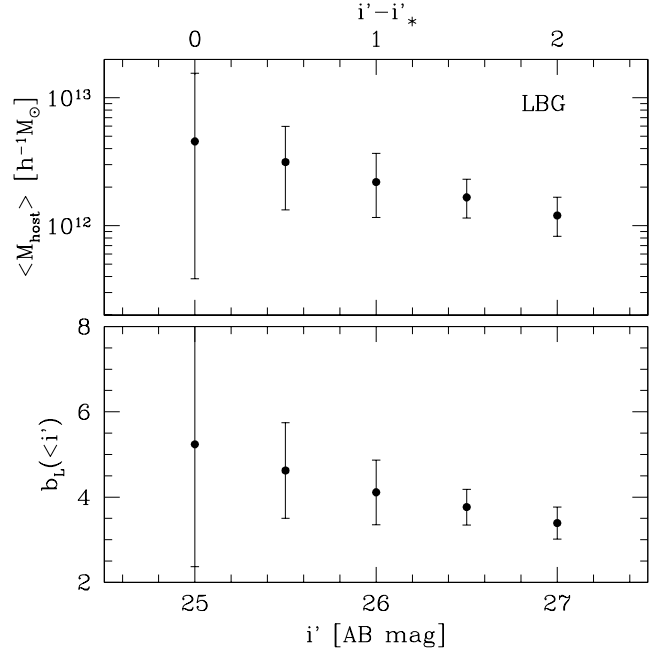
ple is given in Table 1 of Ouchi et al. (2005). The redshift distribution function has the mean of $z \sim 4$ and width of $\Delta z \sim 0.5$ as is shown in the top panels of Figure 12 of Ouchi et al. (2004a). It is found from the spectroscopic follow-up observations for the 63 photometrically-selected LBGs that the 60 objects lie between $z = 3.5$ and 4.5 (Ouchi et al. 2005 and references therein). The contamination fraction is thus estimated to be $f_C = 0.05 (= [63 - 60]/63)$. Ouchi et al. (2004a) computed the luminosity function of the LBGs selected from the Subaru Deep field with the same colour selection criteria and have found $i'_* = 25.0 \pm 0.1$.

The angular two-point correlation functions of the LBGs are computed in the same procedure as was done for the OPEGs and are plotted in the top panel of Figure 3. The integral constraint is estimated to be $\sim 7 \times 10^{-3}$ for a single power-law model with the power-law index of $\beta = -0.8$, we may thus ignore an effect of a finite field size as far as $\theta < 5'$ is concerned. The galaxy bias defined by equation (8) is plotted in the bottom panel. A transition from the small-scale decreasing part to the large-scale flat part is found at the scale of ~ 10 arcsec (see Ouchi et al. 2005 for further detail discussions on the shape of the bias function. Note that they do not correct for the effect of the contamination because of unknown clustering property of the contaminants, for which we assume the random distribution. As a consequence, their measured biases are smaller than ours by about 5 percents). This is transformed to the comoving angular scale of $\sim 0.2 h^{-1} \mathrm{Mpc}$ at $z = 4$, which corresponds to the virial radius of the halo with the mass $\sim 1 \times 10^{12} h^{-1} M_\odot$. This mass, again, coincides with the characteristic mass of hosting haloes ($\langle M_{\mathrm{host}} \rangle$) predicted by the halo model analysis in the next section. Thus the behavior of the bias is understood by the standard halo model picture.

The large-scale bias factor is computed in the same manner as was done for the OPEGs except for using a different separation range of $0.5' < \theta < 5'$ (illustrated in the
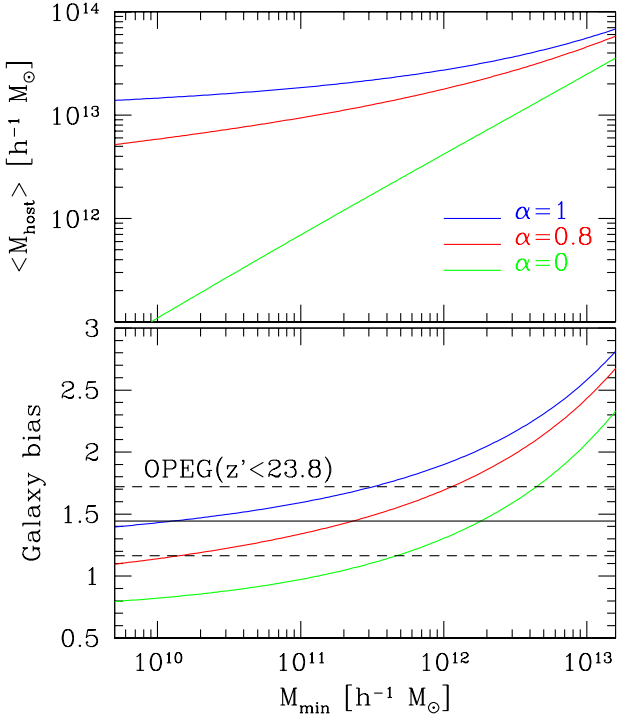
Figure 5. Halo model predictions for OPEGs. *Lower panel*: The large-scale bias $b_{g,L}$ defined by equation (4) for three values of α (1.0, 0.8 and 0 from upper to lower). The horizontal lines show the measured large-scale bias factor for the OPEG sample with $z' < 23.8(= z'_* + 2)$, the solid and dashed line represent the mean and 1-σ range, respectively. *Upper panel*: The mean mass of hosting haloes defined by equation (3) for $\alpha = 1.0$, 0.8 and 0 from upper to lower.

bottom panel of Figure 3). This bias factor is calculated as a function of limiting magnitudes and is plotted in the bottom panel of Figure 4. As was reported by Ouchi et al. (2005), a trend that the large-scale bias factor decreases with the luminosity is observed.

4   RESULTS

We define fiducial subsamples of the two galaxy populations for the later analyses by setting the magnitude limit to 2 magnitude fainter than the m_* value ($z'_* = 21.8$ for the OPEGs and $i'_* = 25.0$ for the LBGs). This is chosen so that it is well deeper than the m_* value and at the same time it is well brighter than the completeness limit of our imaging data ($z' \simeq 26.5$ for the OPEGs and $i' \simeq 27.5$ for the LBGs). The former is imposed so that the samples do not contain only the brightest objects, which would not be representative of the whole population. The latter is imposed to reduce contaminations due to errors in the luminosities and colours. We note that the number densities of the subsamples are $n_{\rm OPEG}(z' < 23.8) = (4.7 \pm 0.47) \times 10^{-3} h^3 {\rm Mpc}^{-3}$ and $n_{\rm LBG}(i' < 27.0) = (1.1 \pm 0.2) \times 10^{-2} h^3 {\rm Mpc}^{-3}$ for OPEGs and LBGs, respectively. Therefore with this selection, the LBGs are as 2.3 times numerous as the OPEGs. It should be noted that statistical properties (e.g., the number density and clustering amplitude) of a galaxy sample would be sensitive to the selection criteria (e.g., the magnitude limit and
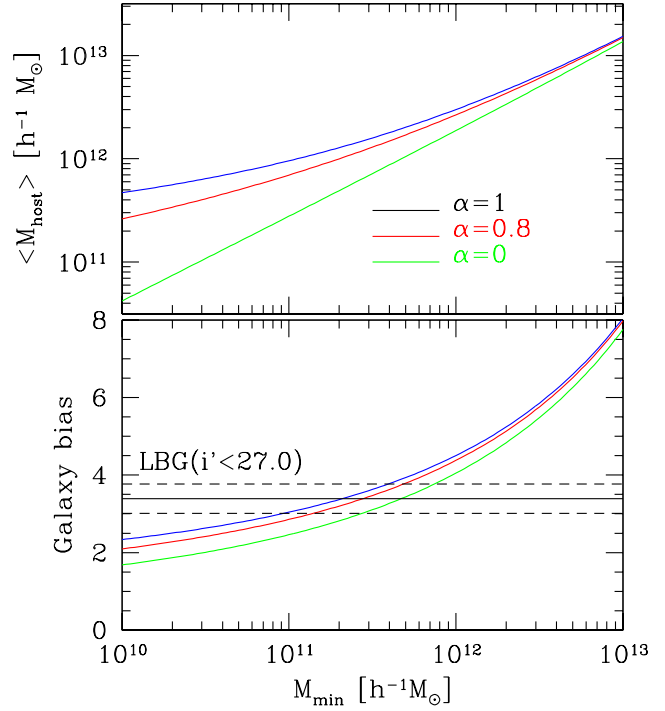
Figure 6. Same as Figure 5 but for the LBGs. Measured large-scale bias factor and number density shown by the horizontal lines are taken from the sample $i' < 27.0(= i'_* + 2)$.

Table 1. Constraints on $\langle M_{\rm host} \rangle$ obtained from the halo model analysis. Unit of the mass is in $[h^{-1} M_\odot]$. [1] values of $\langle M_{\rm host} \rangle$ estimated from the mean of b_L. [2] the interval of $\langle M_{\rm host} \rangle$ from the 1-σ range of b_L.

		mean[1]	1-σ[2]
OPEGs	$\alpha = 1$	1.5×10^{13}	$9.6 \times 10^{12} - 2.2 \times 10^{13}$
($z' < 23.8$)	$\alpha = 0.8$	1.2×10^{13}	$6.3 \times 10^{12} - 1.9 \times 10^{13}$
	$\alpha = 0$	6.6×10^{12}	$2.3 \times 10^{12} - 1.3 \times 10^{13}$
LBGs	$\alpha = 1$	1.3×10^{12}	$9.3 \times 10^{11} - 1.8 \times 10^{12}$
($i' < 27.0$)	$\alpha = 0.8$	1.2×10^{12}	$8.3 \times 10^{11} - 1.7 \times 10^{12}$
	$\alpha = 0$	1.0×10^{12}	$6.4 \times 10^{11} - 1.5 \times 10^{12}$

colour selection). Therefore, when one attempts to compare properties of two (or more) galaxy samples, it is necessary to properly define samples of galaxies with a quantity essential to their nature. In our case, the luminosity would be the most relevant quantity among (a few) controllable parameters we have in hand. Since the definition of our subsamples is based on a somewhat arbitrary magnitude limit, we shall look into an effect of this definition by changing the magnitude limit for subsampling.

4.1   Halo model analyses

We estimate the hosting halo mass by comparing the measured large-scale bias factor with the halo model prediction. To do this, we proceed as follows: First, we compute the halo model prediction for the large-scale bias $b_{g,L}$ defined by equation (4) for a given value of α as a function of M_{min} (plotted in the lower panel of Figures 5 and 6). Then, search-

ing for an interval of M_{min}, where the predicted $b_{g,L}$ and the 1-σ interval of the measured large-scale bias factor intersect, we have a constraint on M_{min}. Since for a given α, $\langle M_{\rm host}\rangle$ and M_{min} have a one-to-one correspondence (see the upper panel of Figures 5 and 6), the constraint on M_{min} is immediately translated into the constraint on $\langle M_{\rm host}\rangle$. We take three values of $\alpha = 1, 0.8$ and 0. Here $\alpha < 1$ is preferred from semi-analytic models of the galaxy formation (e.g., Kravtsov et al. 2004), as well as from the halo model analysis for LBGs (Hamana et al. 2004). We take $\alpha = 0.8$ as a fiducial value. The case $\alpha = 0$ corresponds to an extreme case where every halo with a mass greater than M_{min} always has one galaxy.

    The constraints obtained for our fiducial galaxy samples ($z' < 23.8$ for the OPEGs and $i' < 27.0$ for the LBGs) are summarized in Table 1. It is important to notice that the change in α does not make a significant change in the preferred interval of $\langle M_{\rm host}\rangle$ except for the extreme case of $\alpha = 0$ for the OPEGs. Therefore , the constraint is not very sensitive to the uncertainty in α.

    Let us look into how the characteristic hosting halo mass varies with the limiting magnitude for the sample selection. The upper panels of Figures 2 and 4 show the constraint on $\langle M_{\rm host}\rangle$ as a function of the limiting magnitude. In both galaxy populations, a trend of decreasing $\langle M_{\rm host}\rangle$ for a fainter limiting magnitude is observed. These similar-looking trends, however, may arise from different physical origins as explained below. First, for the OPEGs, the observed z'-band corresponds approximately to the rest-frame B-band. Although the B-band luminosity is affected by ongoing/recent star formation, only a weak star formation activity would make the colour of galaxy blue and pushes it outside of our OPEG selection criteria (Yamada et al. 2005). Therefore the B-band luminosity is a good measure of the stellar mass of the OPEGs. Accordingly, the observed trend is considered as a result of a correlation between the stellar mass and the hosting halo mass. On the other hand, for the LBGs, the observed i'-band corresponds to ~1500Å in the rest-frame, where the luminosity is most sensitive to the star formation. The LBGs are generally in an active star formation phase, also it was reported that the stellar mass of LBGs is poorly correlated with the UV luminosity (Shapley et al. 2001). Therefore, the observed luminosity dependence of hosting halo mass of LBGs may suggest a presence of a correlation between the hosting halo mass and the star formation activity.

4.2   EPS model analyses

We use the conditional mass function $n_2(M_{t2}, z_2|M_{t1}, z_1)$ (equation 7) derived from the EPS formalism to predict the mass evolution of hosting haloes in the framework of the CDM cosmology. For the parameters of the haloes at earlier epoch z_1, we take the 1-σ interval of $\langle M_{\rm host}\rangle$ obtained from the halo model analysis with $\alpha = 0.8$ as a range of M_{t1}, and we set $z_1 = 4$ and $z_1 = 1$ for the LBGs and OPEGs, respectively. Then for a certain later epoch z_2, we compute $n_2(M_{t2}, z_2|M_{t1}, z_1)$ as a function of M_{t2} (see inserts of Figures 7–9 for examples). Assuming that the mass assembly history of hosting haloes is not biased toward any specific merging path, the conditional mass function can be regarded as the probability distribution function (PDF) of the mass of descendant haloes M_{t2}. We define a 68% confidence in-
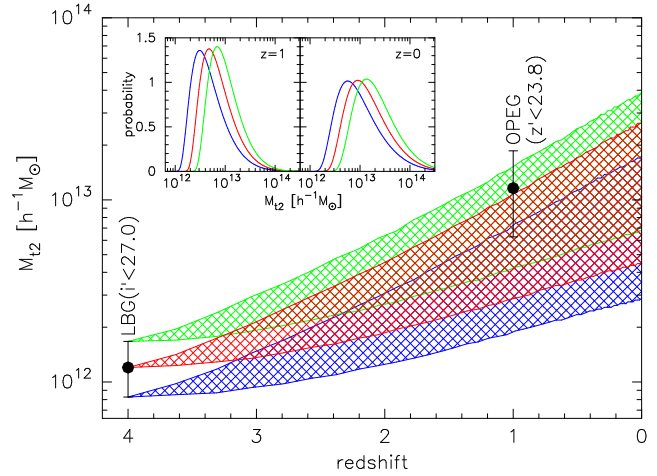

Figure 7. Inserts show arbitrary normalized conditional mass functions $n_2(M_{t2}, z_2|M_{t1}, z_1)$ for $z_2 = 1$ (left panel) and 0 (right panel), where parameters of the earlier halo is taken from the limit obtained by the halo model analysis of the LBGs (with $\alpha = 0.8$): $z_1 = 4$, $M_{t1} = 1.2 \times 10^{12}h^{-1}M_\odot$ (red), 8.3×10^{11} (blue), and 1.7×10^{12} (green). These conditional mass functions are considered as the probability distribution function of the mass of the descendant. The main plot shows 68% confidence intervals of M_{t2} as a function of the redshift (z_2). Three intervals shown by coloured hatches are for the same three M_{t1} values as the inserts. Filled circles with error bars show the limits of $\langle M_{\rm host}\rangle$ obtained from the halo model analysis (with $\alpha = 0.8$) for the LBGs and OPEGs.

terval of M_{t2} as the EPS model prediction for the mass of the descendant halo.

    Such predictions are made for our LBGs and OPEGs samples. and are shown in Figures 7–9 as hatched regions. Three tracks correspond to the three different values of M_{t1} taken from the mean and upper/lower 1-σ values for the $\langle M_{\rm host}\rangle$ denoted by the symbols with error bars ($\alpha = 0.8$ cases in Table 1). The inserts show the PDFs of M_{t2} at $z = 0$ (and $z = 1$). It is observed in the inserts that the PDFs have a wide spread, implying a wide variety of the mass assembly history of hosting haloes. We note that since the PDFs are skewed toward a larger mass, the mean of the distribution is greater than the mode.

    Let us look closely at each result. First of all, Figure 7 compares the expected descendant mass of hosting haloes of the LBGs with the $\langle M_{\rm host}\rangle$ of OPEGs. Both galaxy samples are selected with our fiducial magnitude limit of $m < m_* + 2$. As is evidently shown, the EPS predictions for the mass of the LBG descendant are slightly smaller than the predicted mass range of the OPEGs, only the track from the upper limit of the LBG haloes is compatible with the OPEGs.

    Is there a selection criterion for LBGs or for OPEGs which results in a better agreement? It is found from the upper panel of Fig. 2 that choosing a fainter limiting magnitude for the OPEG sample lowers the $\langle M_{\rm host}\rangle$ very little and can hardly solve the incompatibility. On the other hand, choosing a brighter limiting magnitude for the LBG sample raises the $\langle M_{\rm host}\rangle$ as shown in the upper panel of Figure 4. Indeed, the galaxy sample selected with $i' < 26.0 (= i'_* + 1)$ results in a very compatible halo mass with the $\langle M_{\rm host}\rangle$ of the OPEGs (with $z' < 23.8$) as shown in Figure 8. Therefore, in the view of the mass evolution of hosting haloes, it
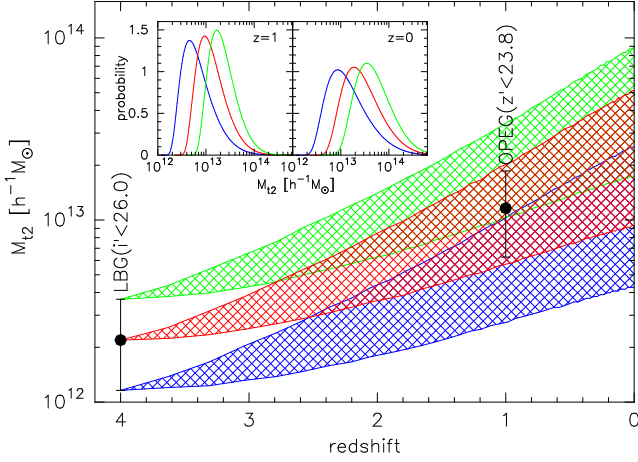
Figure 8. Same as Figure 7 but the LBGs sample is selected with $i' < 26.0$. The limit of $\langle M_{\rm host}\rangle$ obtained from the halo model analysis with $\alpha = 0.8$, which is taken by M_{t1}, is $M_{t1} = 2.2 \times 10^{12}h^{-1}M_\odot$ (red), 1.2×10^{12} (blue), and 3.7×10^{12} (green).
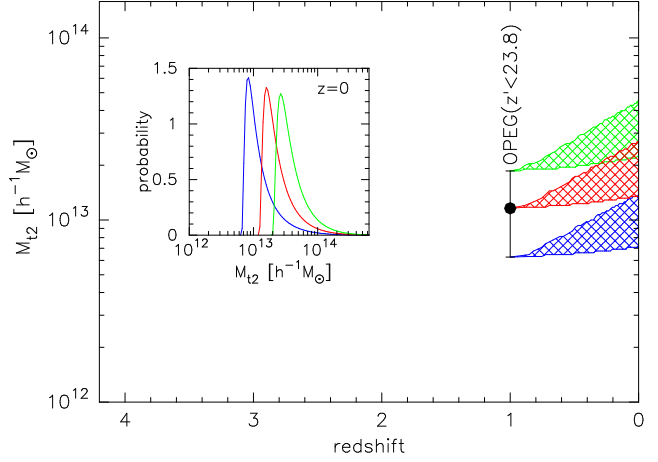

Figure 9. Same as Figure 7 but the limit for OPEGs obtained from the halo model analysis (with $\alpha = 0.8$) is taken by parameters of the earlier halo: $z_1 = 1$, $M_{t1} = 1.2 \times 10^{13}h^{-1}M_\odot$ (red), 6.3×10^{12} (blue), and 1.9×10^{14} (green). In the insert, z_2 is taken by 0.

may be safely concluded that the bright $(i' \lesssim i'_* + 1)$ LBGs are consistent with being the progenitor of the OPEGs, whereas it seems less likely that the LBGs population, as a whole, has evolved into the OPEG population. Note that the corresponding number density is computed to be $n_{\rm LBG}(i' < 26.0) \simeq (3.8 \pm 0.3) \times 10^{-3}h^3{\rm Mpc}^{-3}$, closer to the number density of $n_{\rm OPEG}(z' < 23.8)$.

4.3   Predictions for the present-day descendants

Turn next to predictions for the present-day descendants of the two galaxy populations plotted in Figures 7–9. As is shown in the inserts of Figures 7 and 8, the PDF of the present-day descendants of the LBGs have a very broad spread due to the wide variety of the mass assembly history over $\sim 8h^{-1}$Gyrs. The predicted mass range for the LBG sample with $i' < 27.0$ is broadly consistent with that of the OPEGs, though the PDF of the LBGs extends to a smaller mass (say $M < 10^{13}h^{-1}M_\odot$) where the PDF of the OPEGs has little probability. On the other hand, the predicted mass range for the LBG sample with $i' < 26.0$ agrees better with that of the OPEG descendants. In this case, both the PDFs computed from the central $\langle M_{\rm host}\rangle$ value (the middle one of the three cases in the inserts) peak at $\sim 2 \times 10^{13}h^{-1}M_\odot$, which corresponds to the mass scale of groups of galaxies. It is important to note that since the PDFs are skewed strongly toward a larger mass, a certain fraction of haloes is expected to evolved into more massive haloes with $M_{t2} \gtrsim 10^{14}h^{-1}M_\odot$ (see the inserts of Figures 8 and 9).

It is interesting to compare those EPS predictions for the halo masses of the present-day descendants with local galaxy samples. Since both the LBGs and OPEGs are frequently argued as the strong candidates for the progenitor of the present-day early-type galaxies, we take two clustering analyses of the early-type galaxy samples: One from the the 2dF (Madgwick et al. 2003), and the other from the SDSS (Zehavi et al. 2002). Madgwick et al. (2003) found $\sigma_8^{\rm NL} \simeq 1.1 \pm 0.1$ for "passive" galaxies, of which the luminosity range is $-16.5 < M_{b_J} - 5\log h < -22$ with $M_{b_J,*} = -19.7$. Here $\sigma_8^{\rm NL}$ is the RMS of counts of galaxies
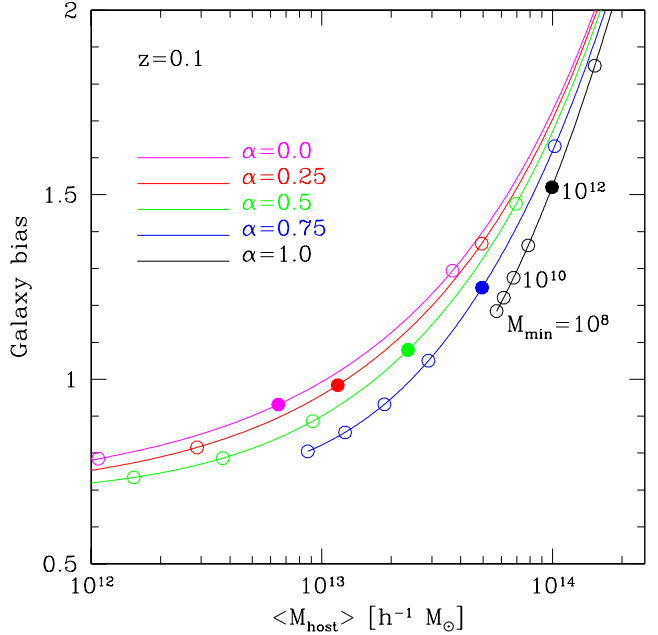

Figure 10. The halo model prediction for the large-scale galaxy bias $b_{g,L}$ as a function of the averaged halo mass $\langle M_{\rm host}\rangle$ at $z = 0.1$. Curves are for a different value of α ($\alpha = 0, 0.25, 0.5, 0.75$ and 1 from upper to lower). Open circles indicate a corresponding value for M_{min} in intervals of $\Delta \log M_{min} = 1$ staring from $M_{min} = 10^8 h^{-1}M_\odot$ with $M_{min} = 10^{12}h^{-1}M_\odot$ being marked by the filled circles.

in spheres of $8h^{-1}$Mpc radius and is derived from the best-fitting power-law model of the real-space correlation function $\xi = (r_0/8)^\gamma$ via the relation $(\sigma_8^{\rm NL})^2 = J_2(\gamma)(r_0/8)^\gamma$ with $J_2(\gamma) = 72/[(3-\gamma)(4-\gamma)(6-\gamma)2^\gamma]$ (Peebles 1980). Since $\sigma_8^{\rm NL}$ of the dark matter is $\sigma_8^{\rm NL} \simeq 0.9$ at $z = 0.1$ (the mean redshift of the galaxy samples considered here) for $\sigma_8 = 0.9$ (note that σ_8 is the linearly extrapolated value at $z = 0$), the corresponding bias is found to be $b_{g,L} \simeq 1.2 \pm 0.1$. Following the same procedure, we estimate $\sigma_8^{\rm NL}$ of galaxy samples from

the SDSS. Adopting the best-fitting power-law models given in Table 2 of Zehavi et al. (2002), we find $\sigma_8^{\mathrm{NL}} = 1.2 \pm 0.03$ for their both "red" (defined by $u - r > 1.8$) and "high concentration" ($c = r_{90}/r_{50} > 2.7$) samples, giving $b_{g,L} \simeq 1.3 \pm 0.03$ for $z = 0.1$ (the mean redshift of the samples). The luminosity range of those galaxies is $-22 < M_r - 5\log h < -19$ with $M_{r,*} = -20.8$. Comparing those bias values (i.e., $b_{g,L} = 1.1 - 1.33$) with the halo model predictions plotted in Figure10, we find $\langle M_{\mathrm{halo}} \rangle = (2 - 6) \times 10^{13} h^{-1} M_\odot$ for $0.25 \lesssim \alpha \lesssim 0.75$ (Note that as is shown Figure10, the relation between the large-scale bias and $\langle M_{\mathrm{halo}} \rangle$ only weakly depends on α). This is broadly consistent with the EPS predictions for the descendants of the OPEGs (with $z' < 23.8$) and also with that of the LBGs (with $i' < 26.0$). Therefore, we may conclude that, in the viewpoint of the mass evolution of hosting haloes in the CDM model, the OPEGs and the bright LBGs are consistent with being the progenitor of the present-day early-type galaxies.

5 SUMMARY AND DISCUSSIONS

We have analyzed the two photometrically-selected galaxy samples from the deep mult-band images of the SXDS: the LBGs at $z \sim 4$ and OPEGs at $z \sim 1$. The contiguous large survey area of the SXDS enables us to measure the angular two-point correlation functions over a wide range of separations with a good statistical quality. Comparing the large-scale clustering amplitude with the corresponding halo model predictions, we have estimated a characteristic mass of hosting haloes. Then, adopting the EPS model, we have computed the predictions for the mass evolution of the hosting haloes to explore the likely descendants of those galaxy samples. In particular, we have compared the predicted halo masses of these two populations at different epochs to make a possible evolutionary link. We have also examined expected halo masses of the present-day descendants of those two galaxy populations.

Our major findings are summarized as follows:

(i) The measured bias functions (defined by equation 8) of both the OPEGs and LBGs consist of two parts: The decreasing small-scale part and the flat large-scale part. The transition scales between them are $1'$ and $10''$ for the OPEGs and LBGs, respectively. Those scales agree well with the virial radii of haloes with the characteristic mass of hosting haloes predicted by the halo model analysis in §4. The shape of the bias function is thus understood by the standard halo model picture: The small-scale clustering arises from galaxy pairs located in the same halo, and the large-scale clustering arises from galaxy pairs located in two different haloes.

(ii) The conclusive measurement of the flat large-scale bias allows us to safely define the large-scale bias factor. Also, the large number of galaxies allows us to examine the luminosity dependence of the large-scale bias factor. It is found that the large-scale bias factors of both OPEGs and LBGs positively correlates with the luminosity (see bottom panels of Figures 2 and 4).

(iii) Comparing the measured large-scale bias factors of the two galaxy samples with the halo model predictions, we estimate the characteristic mass of hosting haloes. The merit of using the large-scale bias factor is two-fold: First is concerning the measurement; since many bins are used to compute it, the measurement is less sensitive to a statistical noise in each bin. Second is concerning the halo model; the large-scale bias does not depend on M_1, and in addition, the resultant $\langle M_{\mathrm{halo}} \rangle$ is less sensitive to α. Therefore it provides with a reliable estimate of $\langle M_{\mathrm{halo}} \rangle$. The predicted characteristic halo masses of both galaxy samples are found to be positively correlated with the luminosity. For the OPEGs, this may arise from a correlation between the stellar mass and the hosting halo mass, because the observed z'-band magnitude (rest-frame B-band) is well correlated to the stellar mass for population like OPEGs with little star formation activity. On the other hand, for the LBGs, it may suggest a correlation between the hosting halo mass and the star formation activity, rather than the stellar mass. This is because the observed i'-band corresponds to ~ 1500Å in the rest-frame, where the luminosity is most sensitive to the star formation, and in addition, the LBGs are generally in an active star formation phase.

(iv) Utilizing the EPS model, we compute the predictions for the halo mass distribution of the LBGs' descendants at $z = 1$ in the CDM cosmology, and then we compare it with the halo model prediction for the characteristic halo mass of the OPEGs. It is found that, for our fiducial subsamples (the OPEGs with $z' < 23.8$ and the LBGs with $i' < 27.0$), the typical hosting halo mass of LBGs' descendants is slightly smaller than the predicted mass of the OPEGs' hosting haloes. It is also found that the brighter LBG subsample (with $i' \lesssim 26.0$) is likely to evolve into the systems with halo mass compatible to the predicted one of the OPEGs. Therefore, we may conclude that, in the viewpoint of the mass evolution of hosting haloes in the framework of the CDM model, the bright ($i' \lesssim i'_* + 1$) LBGs are consistent with being the progenitor of the OPEGs. Accordingly, it seems less likely that the LBGs population, as a whole, has evolved into the OPEG population.

(v) We also compute predictions for halo masses of the present-day descendants of both the galaxy samples using the EPS model. It is found that the predicted mass range for the LBG sample with $i' < 27.0$ is slightly but systematically smaller than that of the OPEGs (with $z' < 23.8$). On the other hand, the prediction for the LBG sample with $i' < 26.0$ agrees better with that of the OPEG descendants. In the latter case, the peaks of the PDFs are located at $\sim 2 \times 10^{13} h^{-1} M_\odot$ and the tail of the PDFs extends to the mass range of $M > 10^{14} h^{-1} M_\odot$. Thus the present-day descendants of the bright LBGs and the OPEGs are likely to be located in massive systems such like groups of galaxies or clusters of galaxies. We also estimate the characteristic halo mass of local early-type galaxy samples from the 2dF and SDSS with the halo model, and it turns out that the predicted mass is in good agreement with the EPS predictions for the present-day descendant's mass of both the bright LBGs and OPEGs. Therefore, it is concluded that, in the viewpoint of the mass evolution of hosting haloes in the CDM model, the OPEGs and bright LBGs are consistent with being the progenitor of the present-day early-type galaxies.

One of the most interesting implications from the above findings is that the possible halo mass dependence of the LBG's star formation history. This is speculated from the above finding (iv) that the predicted descendant's halo mass

of bright LBG subsample ($i' \lesssim i'_* + 1$) is found to be in very good agreement with the characteristic halo mass of the OPEGs, whereas it seems less likely that the faint LBG population has evolved into the OPEG population. The nature of the descendants of the faint LBGs at $z \simeq 1$ is not clear but is naively expected that they evolve into other populations than old passively evolving galaxies with lower mass and bluer spectra. It is important to notice that a little star formation at $z < 2$ would be enough to push the galaxy colour outside of the OPEG's colour criteria (Yamada et al. 2005). Therefore, the halo mass dependence of the epoch of truncation in star formation activity is one possibility of interpreting the finding (iv). It is also found that the UV luminosity of the LBGs correlates with the hosting halo mass [the above finding (iii)]. This may be an additional evidence for the mass dependent star formation history, though a connection between the above two findings, (iii) and (iv), is not clear. A possible scenario is that LBGs in more massive haloes have more active star formation at significantly high redshift such as $z \sim 4$, and they turn into the passive evolution phase earlier. This scenario can be tested by performing the same clustering analysis as presented in this paper progressively toward lower (and higher) redshifts. We might be able to see the transition at some point where star formation activities in massive haloes are truncated and the mass of the haloes that are hosting active star formation is being shifted to lower mass as time progresses. At the same time, on the theoretical side, we should explore a possible physical mechanism that drives such mass dependent star formation histories.

Before closing, it is important to note that we have *not* argued that LBGs are the only path to become OPEGs at $z = 1$ or the present-day early-type galaxies. In fact, it is likely that the ancestor–descendant connection is not a one-to-one correspondence, and some different high-z galaxy populations may have evolved into a similar low-z population, and vice versa. For example, among the ancestors of the OPEGs at $z = 1$, there may be some haloes which have not collpased by $z = 4$ and would be seen as LBGs at some later epochs, as well as the objects which are not UV luminous enough to be selected as LBGs at $z = 4$ due to large amount of dust extinction and/or older stellar ages. This is one reason why we have not take into account the number density of our galaxy samples when we examine their possible connection. We note, however, the number density of the bright LBGs $n_{LBG}(i' < 26.0) \simeq 3.8 \times 10^{-3} h^3 \text{Mpc}^{-3}$ is in fact comparable to that of OPEGs $n_{OPEG}(z' < 23.8) \simeq 4.7 \times 10^{-3} h^3 \text{Mpc}^{-3}$. Therefore, we could even argue from this comparison that the bright LBG–OPEG connection could be the major ancestor–descendant relation *if* the number density of bright LBGs would not decrease significantly by mergers.

REFERENCES

Adelberger K. L., Steidel C. C., Pettini M., Shapley A. E., Reddy N. A., Erb D. K., 2005, ApJ, 619, 697
Bardeen J. M., Bond J. R., Kaiser N., Szalay A. S. 1986, ApJ, 304, 15
Bartelmann M., Schneider P., 2001, Phys. Rep., 340, 291
Bond J. R., Cole S., Efstathiou G., Kaiser N., 1991, ApJ, 379, 440
Bower R. G., 1991, MNRAS, 248, 332
Bruzual G., Charlot S., 2003, MNRAS, 344, 1000
Coil A. L., Newnman J. A., Kaiser, N., Davis M., Ma C.-P., Kocevski D. D., Koo D. C., ApJ, 617, 765
Daddi E., Broadhurst T., Zamorani G., Cimatti A., Röttgering H., Renzini A., 2001, A&A, 376, 825
Dressler A., 1980, ApJ, 236, 351
Firth A. E., et al. 2002, 332, 617
Franx M. et al., 2003, ApJ, 587, L79
Giavalisco M., Dickinson M., 2001, ApJ, 550, 177
Groth E. J., Peebles P. J. E., 1977, ApJ, 217, 385
Hamana T., Ouchi M., Shimasaku K., Kayo I., Suto Y., 2004, MNRAS, 347, 813
Kodama T. et al., 2004, MNRAS, 350, 1005
Kravtsov A. V., Berlind A., Wechsler R. H., Klypin A. A., Gottlöber S., Allgood B., Primack J. R., 2004, ApJ, 609, 35
Lacey C., Cole S. 1993, MNRAS, 262, 627
Landy S. D., Szalay A. S., 1993, ApJ, 412, 64
Maggwick et al., 2003, MNRAS, 344, 847
McCarthy P. J., et al. 2001, ApJL, L131
Miyazaki M., et al, 2003, PASJ, 55, 1079
Mo, H. J., White, S. D. M. 1996, MNRAS, 282, 347
Moustakas L. A., Somerville R. S., 2002, ApJ, 577, 1
Ouchi M, et al., 2005, submitted to ApJ, astro, arXiv:astro-ph/0508083
Ouchi M., et al., 2004a, ApJ, 611, 660
Ouchi M., et al., 2004b, ApJ, 611, 685
Peacock J. A., Dodds S. J., 1996, MNRAS, 280, L19
Peebles P. J. E., 1980, The Large-Scale Structure of the Universe Princeton Univ. Press, Princeton, NJ
Postman M., Geller M. J., 1984, ApJ, 281, 95
Press W. H., Schechter P., 1974, ApJ, 187, 425
Reddy N. A., Erb D. K., Steidel C. C., Shapley A. E., Adelberger K. L., Pettini M., 2005, ApJ, in press (astro-ph/0507264)
Roche N. R., Almaini O., Dynlop J., Ivison R. J., Willott C. J., 2002, MNRAS, 337, 1282
Shapley A. E., Steidel C. C., Adelberger K. L., Dickinson M., Giavalisco M., Pettini M., 2001, ApJ, 562, 95
Sheth R. K., Tormen G., 1999, MNRAS, 308, 119
Yamada T., et al, 2005, ApJ, in press
Zehavi I., et al, 2002, ApJ, 571, 172